Shedding Light on Zwitterionic Magnetic Nanoparticles: Limitations for *in vivo* Applications.

Manuel Pernia Leal[§,†,*], Carlos Caro[§,†], María Luisa García-Martín[§,#,*].

[§]BIONAND, Andalusian Centre for Nanomedicine and Biotechnology, Universidad de Málaga, 29590 Málaga, Spain.

[†]Departamento de Química Orgánica y Farmacéutica, Universidad de Sevilla, 41012 Seville (Spain).

[#]Networking Research Centre on Bioengineering, Biomaterials and Nanomedicine, CIBER-BBN, 29590 Malaga, Spain.

Index

7. In vivo pharmacokinetics after MNP administration

8. Histology of mouse renal cortex after MNP injection.

1. *Synthesis of manganese ferrite* nanoparticles *(MNPs)*.

MNPs were synthesized following the protocol previously described.[1] Briefly, in a 50 mL two-necked round-bottom flask 2 mmol of iron acetylacetonate, 1 mmol of manganese acetylacetonate, 10 mmol of hexadecanediol, 6 mmol of dodecylamine, 6 mmol of oleylamine and 20 mL of benzyl ether were mixed and magnetically stirred under a flow of nitrogen. The mixture was heated to 110 °C for 1 h, then the solution was heated at a rate of 3.3 ºC/min to 210 ºC for 2 h, followed by increasing the temperature to reflux (300 °C) for 1 h. The mixture was cooled down to room temperature. Finally, the nanoparticles were precipitated two times using a mixture of acetone and isopropanol (1:1) as precipitation agents, centrifuged (10 min at 4000 rpm) followed by re-dispersion in toluene.

The purified manganese ferrite nanoparticles were characterized by transmission electron microscope (TEM), as shown in Figure S1. The average diameter of the nanoparticle core was calculated by measuring on at least 100 nanoparticles to be 6.9 ± 0.7 nm.

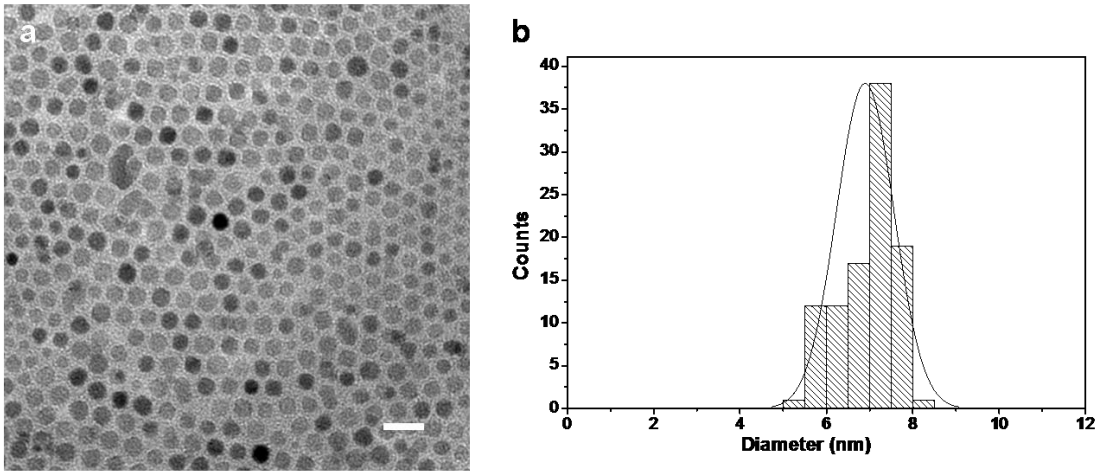

Figure S1. a) Representative TEM image of the manganese ferrite nanoparticles. Scale bar corresponds to 20 nm. b) the corresponding histograms of the TEM diameter of the inorganic core measured on at least 100 nanoparticles.

2. Synthesis of ligands:

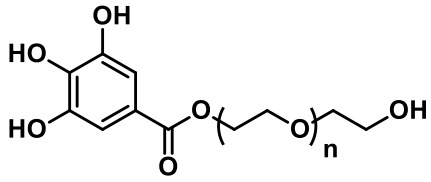

The gallol-PEGn-OH was synthesized following the previously synthetic route reported by us.[2] In brief, to a solution of poly ethylene glycol (Mw: 3000 g/mol, 1 mmol, 3.0 g), gallic acid (Mw: 170 g/mol, 1 mmol, 170 mg) and 4-(dimethylamino) pyridine (Mw: 122 g/mol, 200 μmol, 24 mg) in 100 mL of tetrahydrofuran and 10 mL of dichloromethane, in a round-bottom flask under nitrogen atmosphere, was added dropwise a solution of dicyclohexyl carbodiimide (Mw: 206 g/mol, 5 mmol, 1 g). The mixture was stirred overnight at room temperature. The reaction mixture was filtered through a filter paper and solvents were rota-evaporated. The crude product was dissolved in 100 mL of milli-Q water and the solution was adjusted to pH 2 by adding few mL of a 0.1 mM HCl solution. The product was extracted from the water phase with dichloromethane (100 mL, three times). The organic layer was dried over Na_2SO_4, filtered through a filter paper and the solvent was rota-evaporated. ^{1}H NMR spectroscopy confirmed the desired product gallol-PEG-OH. ^{1}H NMR (400 MHz, $CDCl_3$) δ (ppm): 7.22 (s, 2H), 4.43-4.40 (m, 2H), 3.85-3.45 (m, CH_2-PEG, -OH). FTIR peaks (cm^{-1}): 1466 (C-H bend vibration), 1359 (C-H bend vibration), 1341 (C-H bend vibration), 1307 (anti-symmetric stretch vibration), 1268 (C-O stretch vibration), 1238

(C-O stretch vibration), 1092 (C-O-C stretch vibration), 942 (CH out-of-plane bending vibration).

Synthesis of gallol-PEGn-NH_2

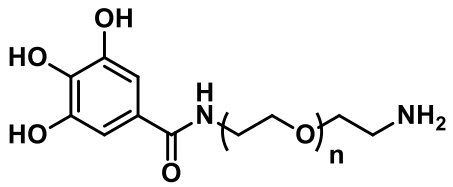

The gallol-PEG-NH_2 was synthesized following the same procedure commented above. Briefly, to a solution of α,ω Bis-amino-poly ethylene glycol (Mw: 3000 g/mol, 0.67 mmol, 2.0 g), gallic acid (Mw: 170 g/mol, 0.67 mmol, 114 mg) and 4-(dimethylamino) pyridine (Mw: 122 g/mol, 134 μmol, 16 mg) in 100 mL of tetrahydrofuran and 10 mL of dichloromethane, in a round-bottom flask under nitrogen atmosphere, was added dropwise a solution of dicyclohexyl carbodiimide (Mw: 206 g/mol, 3.35 mmol, 690 mg). The mixture was stirred overnight at room temperature. The reaction mixture was filtered through a filter paper and solvents were rota-evaporated. The crude product was dissolved in 100 mL of milli-Q water and the solution was adjusted to pH 2 by adding few mL of a 0.1 mM HCl solution. The product was extracted from the water phase with dichloromethane (100 mL, three times). The organic layer was dried over Na_2SO_4, filtered through a filter paper and the solvent was rota-evaporated. ^{1}H NMR spectroscopy confirmed the desired product gallol-PEG-NH_2. ^{1}H NMR (400 MHz, $CDCl_3$) δ (ppm): 7.22 (s, 2H), 4.43-4.40 (m, 4H), 3.85-3.45 (m, CH_2-PEG). FTIR peaks (cm^{-1}): 1650 (C-N stretch vibration), 1615 (N-H bend and C-N stretch vibrations), 1466

(C-H bend vibration), 1359 (C-H bend vibration),1341 (C-H bend vibration), 1307 (anti-symmetric stretch vibration), 1268 (C-O stretch vibration), 1238 (C-O stretch vibration), 1092 (C-O-C stretch vibration), 942 (CH out-of-plane bending vibration).

Synthesis of gallol-PEGn-NMe$_2$

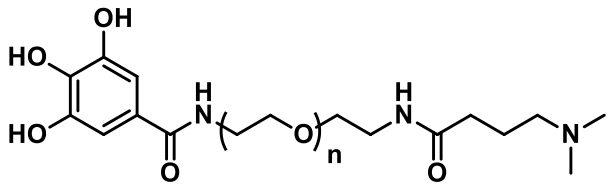

The incorporation of the dimethylamino to the gallol derived was synthesized following a modified protocol previously published.[3] To a solution of gallol-PEG-NH_2 (Mw: 3152 g/mol, 0.67 mmol, 2.1 g), 4-(dimethylamino) butyric acid hydrochloride (Mw: 168 g/mol, 1 mmol, 168 mg), Et_3N (Mw: 101.1 g/mol, ρ = 0.726 g/mL, 1 mmol, 280 μL) in 20 mL of $CHCl_3$ under a nitrogen flow and ice-cold conditions was added dropwise a solution of dicyclohexyl carbodiimide (Mw: 206 g/mol, 1 mmol, 206 mg) and 4-(dimethylamino) pyridine (Mw: 122 g/mol, 300 μmol, 36 mg) in 10 mL of $CHCl_3$. The mixture was left stirred overnight at room temperature under N_2 atmosphere. The mixture was filtered through a filter paper and the organic layer was washed with water (30 mL, two times) and with saturated Na_2CO_3 solution (30 mL, two times). The $CHCl_3$ layer was dried over Na_2SO_4, filtered through a filter paper and rota-evaporated. ^{1}H NMR spectroscopy confirmed the desired product. ^{1}H NMR (400 MHz, D_2O) δ (ppm): 8.05 (s, 1H), 7.68 (s, 2H), 6.76 (s, 1H), 3.90-3.52 (m, CH_2-PEG), 3.41-3.39 (m, 4H), 3.10-3.07 (m, 2H), 2.44-2.27 (m, 8H), 1.87-1.80 (m, 2H). FTIR peaks (cm^{-1}): 1650 (C-

N stretch vibration), 1615 (N-H bend and C-N stretch vibrations), 1466 (C-H bend vibration), 1359 (C-H bend vibration), 1341 (C-H bend vibration), 1307 (anti-symmetric stretch vibration), 1268 (C-O stretch vibration), 1238 (C-O stretch vibration), 1092 (C-O-C stretch vibration), 942 (CH out-of-plane bending vibration).

Synthesis of gallol-PEGn-Zw

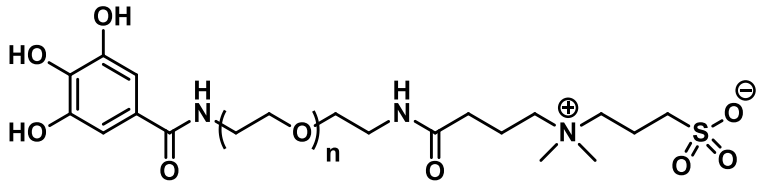

The gallol derived Zwitterionic was synthesized following a modified protocol previously published.[3] Gallol-PEG-NMe_2 (Mw: 3265 g/mol, 0.31 mmol, 1.0 g) and 1,3-propanesultone (Mw: 122 g/mol, 0.34 mmol, 41.6 mg) were dissolved in 30 mL of $CHCl_3$. The mixture was left stirred under nitrogen atmosphere at room temperature for three days. Then, the $CHCl_3$ was rota-evaporated, and the crude product was washed with ethyl acetate (60 mL, three times). ^{1}H NMR spectroscopy confirmed the desired product. ^{1}H NMR (400 MHz, D_2O) δ (ppm): 8.02 (s, 1H), 7.68 (s, 2H), 6.90 (s, 1H), 4.28-3.57 (m, CH_2-PEG), 3.56-3.50 (m, 2H), 3.43-3.35 (m, 4H), 3.13 (m, 6H), 3.03-2.97 (m, 2H), 2.94-2.90 (m, 2H), 2.53-2.47 (m, 2H), 2.41-2.36 (m, 2H), 2.32-2.19 (m, 2H). FTIR peaks (cm^{-1}): 1650 (C-N stretch vibration), 1615 (N-H bend and C-N stretch vibrations), 1466 (C-H bend vibration), 1359 (C-H bend vibration), 1341 (C-H bend vibration), 1307 (anti-symmetric stretch vibration), 1268 (C-O stretch vibration), 1238

(C-O stretch vibration), 1092 (C-O-C stretch vibration), 1036 (S-O stretch vibration), 942 (CH out-of-plane bending vibration).

3. Functionalization of manganese ferrite nanoparticles

The functionalization of the MNPs were performed following the previously protocol published.[2, 4] Briefly, in a separating funnel was added a solution of 1.0 mL of manganese ferrite nanoparticles (10 g/L of Fe, Mn), 1.0 mL of the corresponding gallol-PEGn derived: neutral (OH), positive (NMe_2) or zwitterionic (Zw) in a concentration of 0.1 M in $CHCl_3$ and 50 mL of triethylamine. The mixture was shaked gently and it was diluted with 5 mL of toluene, 5 mL of milli-Q water and 10 mL of acetone. Then, it was shaken and the manganese ferrite nanoparticles were transferred into the aqueous phase. After that, the aqueous phase was collected in a round-bottom flask and the residual organic solvents were rota-evaporated. Then, the gallol derived MNPs were purified in centrifuge filters with a molecular weight cut-off of 100 kDa at 450 rcf. In each centrifugation, the functionalized MNPs were re-suspended with milli-Q water. The purification step was repeated several times until the filtered solution was cleared. Then, the gallol derived MNPs were re-suspended in PBS buffer. Finally, to ensure high stable mono-dispersed magnetic nanoparticles, the solution of MNPs was centrifuged at 150 rcf for 5 min and also, it was placed onto a permanent magnet (0.6 T) for 5 min.

4. Physico-chemical characterization of the gallol derived MNPs.

The neutral (gallol-PEG3kDa-OH), positive (gallol-PEG3kDa-NMe_2) and zwitterionic (gallol-PEG3kDa-Zw) manganese ferrite nanoparticles were characterized through different physico-chemical techniques.

The presence of the gallol ligands attached to the surface of the nanoparticle was analyzed by FTIR spectroscopy and thermo-gravimetric analysis.

Figure S2 shows the FTIR spectrum of each ligand. The main difference between gallol-PEG-OH and gallol-PEG-NMe_2 is the appearance of two peaks at 1650 cm^{-1}, which is assigned to C-N stretching vibration, and at 1615 cm^{-1}, assigned to N-H bending and C-N stretching vibrations. The further modification of gallol-PEG-NMe_2 to gallol-PEG-Zw promotes a change in the relative intensities of the peaks 1650 cm^{-1} and 1615 cm^{-1}. The intensity of the peak 1615 cm^{-1} decreases in favor of the peak 1650 cm^{-1}, since the tertiary amine group reacts with the 1,3-propanesultone. The remaining peak at 1615 cm^{-1} could be due to a small contribution of C-N stretching vibrations, and the increase of the intensity of the peak 1650 cm^{-1} could be due to the formation of a new C-N bond between the tertiary amine and the 1,3-propanesultone. In addition, the appearance of a peak at 1036 cm^{-1} in the gallol-PEG-Zw can be assigned to the stretching vibration of the S-O bonds in the $-SO_3$ groups, thus confirming the attaching of the sultone to the gallol-PEG-NMe_2. After the functionalization of the nanoparticles with the different ligands, the FTIR spectra do not show any substantial difference between the free ligand and the functionalized nanoparticles.

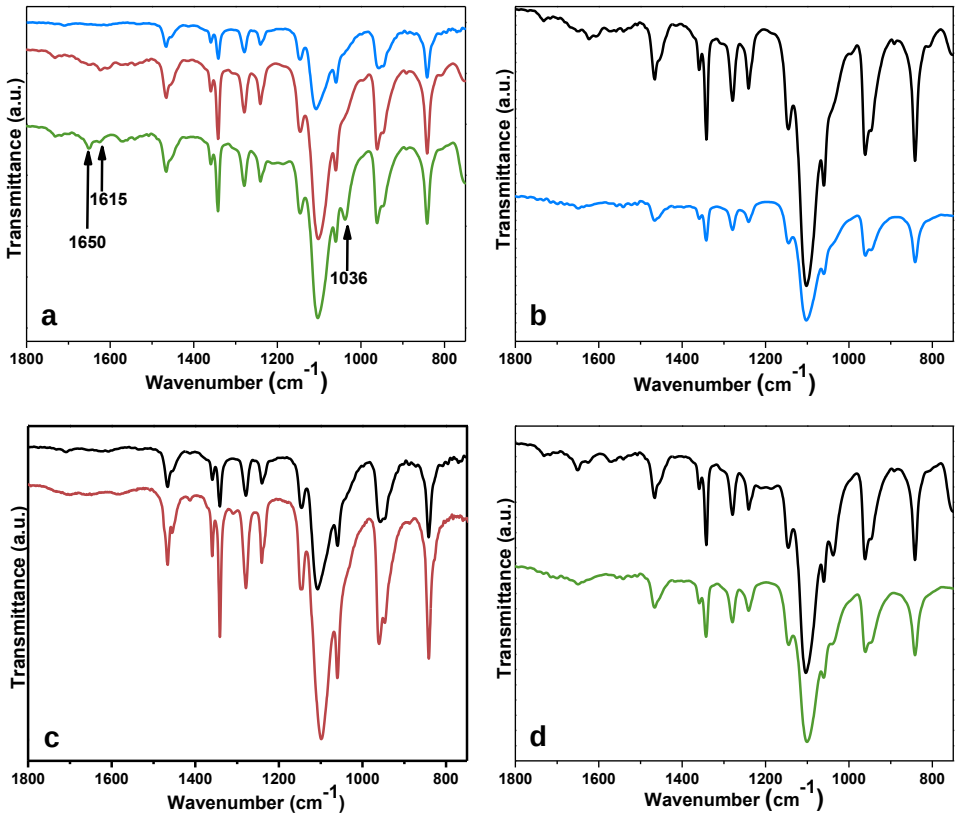

Figure S2. a) FTIR spectra of the ligands: blue curve (gallol-PEG3kDa-OH), red curve (gallol-PEG3kDa-NMe_2) and green curve (gallol-PEG3kDa-Zw); b) FTIR spectra of ligand gallol-PEG3kDa-OH (black curve) and MNP-gallol-PEG3kDa-OH (blue curve); c) FTIR spectra of ligand gallol-PEG3kDa-NMe_2 (black curve) and MNP-gallol-PEG3kDa- NMe_2 (red curve) and d) FTIR spectra of ligand gallol-PEG3kDa-Zw (black curve) and MNP-gallol-PEG3kDa-Zw (green curve).

The percentage of the organic layer on the manganese ferrite nanoparticles was quantified by thermo-gravimetric analysis giving values of 54%, 74% and 83% for the neutral, positive and zwitterionic MNPs, respectively.

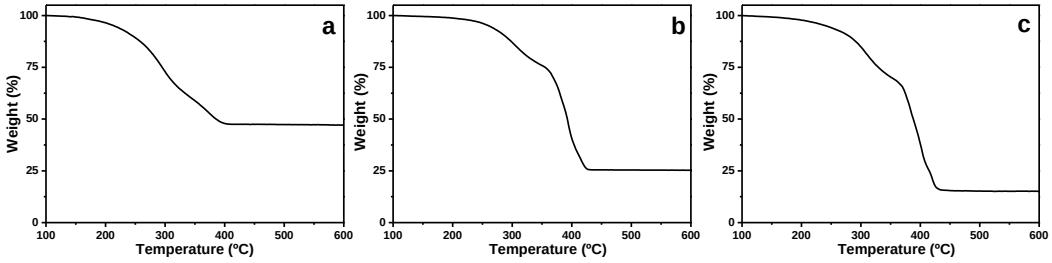

Figure S3. Thermo-gravimetric analysis of a) MNP-gallol-PEG3kDa-OH; b) MNP-gallol-PEG3kDa-NMe_2 and c) MNP-gallol-PEG3kDa-Zw.

Furthermore, the dispersant packing density of the different charged magnetic nanoparticles was calculated based on the TGA and TEM results. So the number of molecules of gallol-PEG3kDa-OH per nm^2 of MNP was determined as follows:

Molecular weight of gallol-PEG3kDa-OH: 3152 g/mol

Radius of the manganese ferrite nanoparticle: 3.45 nm

By thermo-gravimetric analysis: 46% inorganic nanoparticle and 54% organic material

$$\rho = \frac{Total\ number\ of\ molecules\ of\ ligand}{S_{Total\ NP}\ (nm^2)}$$

$$S_{Total\ NP} = {}_{N_{NP}} \times S_{NP} = 783.75 \cdot 10^{17} nm^2$$

$$S_{Total\ NP} = 4\pi r^2 = 149.57\ nm^2$$

$$d_{NP(Fe2MnO4)} = 5.1\ g/cm^3$$

$$m_{NP} = {}_{d_{NP}} \times V_{NP} = 877.5 \cdot 10^{-21} g$$

$$V_{NP} = \frac{4}{3}\pi r^3 = 172.06\ nm^3$$

$$m_{Total\ NP} = {}_{m_{NP\ by\ TGA}} = 0.46\ g$$

$$Total\ number\ of\ molecules\ of\ ligand = \frac{m_{organic\ by\ TGA}}{Mw_{ligand}} \times N_A = 1.03 \cdot 10^{20}$$

$$N_{NP} = m_{Total\ NP} \times m_{NP} = 5.24 \cdot 10^{17}$$

$$\boldsymbol{\rho} = \frac{Total\ number\ of\ molecules\ of\ ligand}{S_{Total\ NP}\ (nm^2)} = \frac{1.03\ 10^{20}\ \text{molecules of ligand}}{783.75 \cdot 10^{17} nm^2}$$

$$= \mathbf{1.3\ molecules\ of\ gallol - PEG3kDa - OH\ per\ nm^2}$$

The packing density for the gallol-PEG3kDa-NMe_2 onto the magnetic nanoparticles with Mw = 3265 g/mol, inorganic mass of 26% and 74% of organic mass, was calculated as showed above, obtaining a **ρ = 3.1 molecules of ligand per nm^2.**

And, for the gallol-PEG3kDa-Zw onto the MNP (Mw= 3387 g/mol, 17% of inorganic mass and 83% of organic mass) it was obtained a **ρ = 5.1 molecules of ligand per nm^2.**

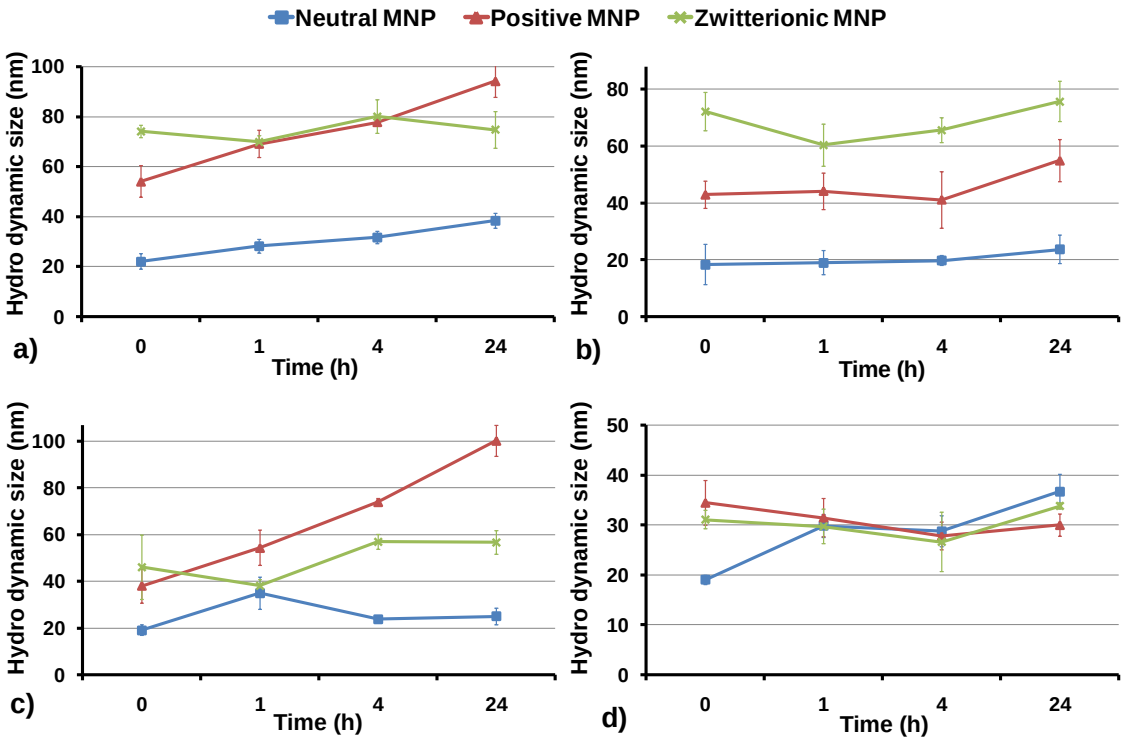

Figure S4. Hydrodynamic diameters of neutral, positive and zwitterionic manganese ferrite nanoparticles vs time at 37ºC in (a) water; (b) PBS buffer; (c) cell growth medium and (d) blood plasma.

Z-potential measurements: The different MNPs (neutral, positive and zwitterionic) suspensions were dispersed in water at the desired pH values (5, 6, 7 and 8), the final concentration being 50 mg of MNPs/L. The zeta potential measurements were performed on the Zetasizer at 0, 24 and 48 h.

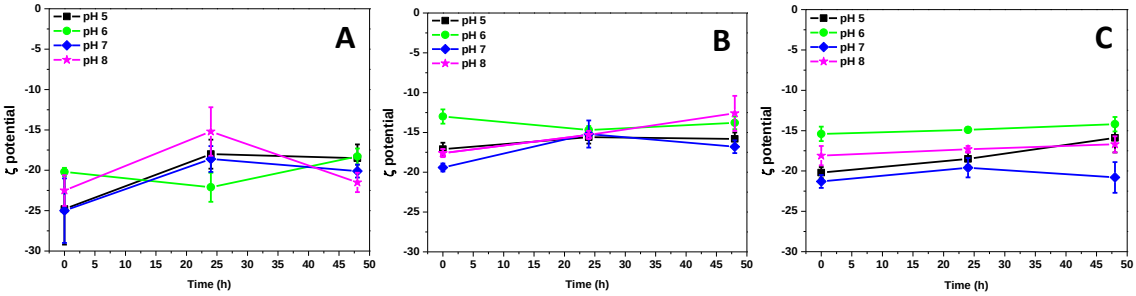

Figure S5. Zeta potential measurements vs time and pH of neutral (a), positive (b), and zwitterionic (c) MNPs.

The longitudinal and transverse relaxivities, r_1 and r_2, were determined at clinical and pre-clinical magnetic fields (1.5 and 9.4 T).

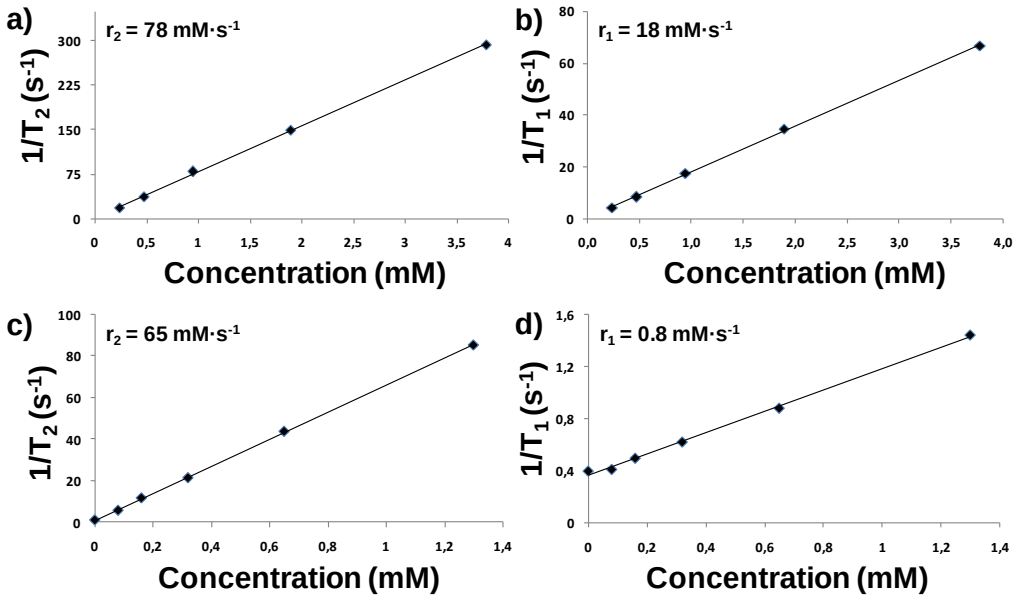

Figure S6. Plot of 1/T over Fe, Mn concentration of neutral manganese ferrite nanoparticles: a) and b) transverse and longitudinal relaxivities at 1.5 T; c) and d) transverse and longitudinal relaxivities at 9.4 T.

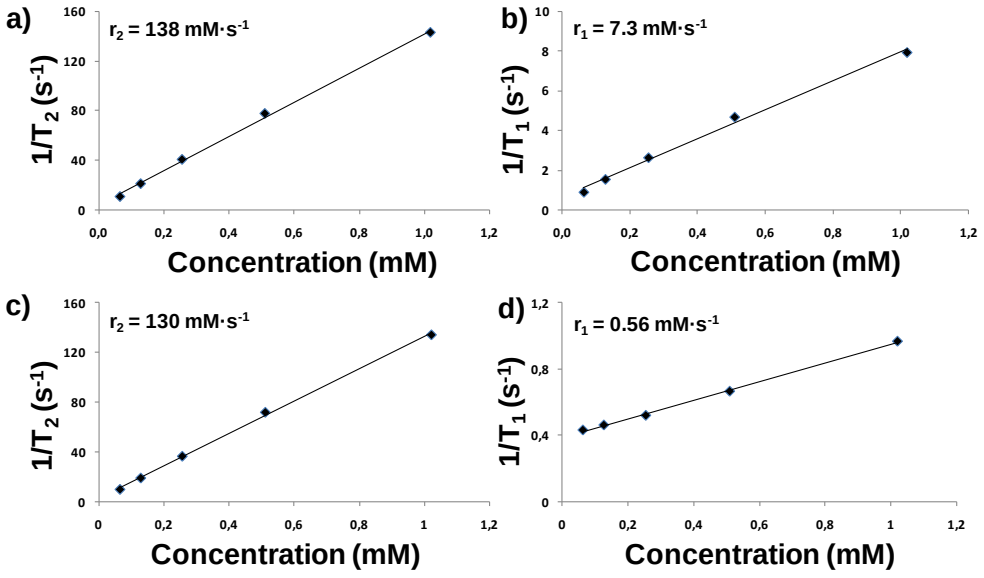

Figure S7. Plot of 1/T over Fe, Mn concentration of positive manganese ferrite nanoparticles: a) and b) transverse and longitudinal relaxivities at 1.5 T; c) and d) transverse and longitudinal relaxivities at 9.4 T.

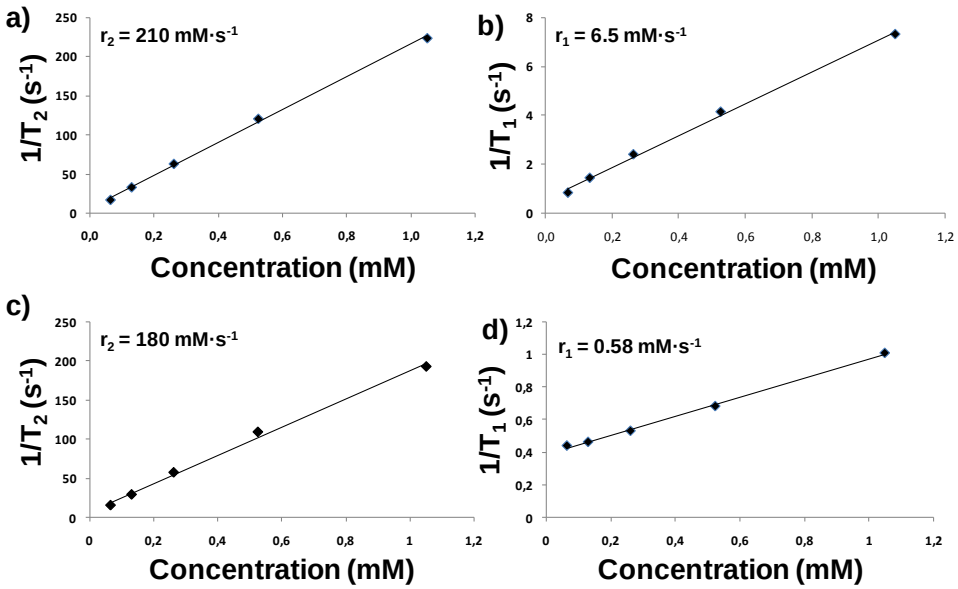

Figure S8. Plot of 1/T over Fe, Mn concentration of zwitterionic manganese ferrite nanoparticles: a) and b) transverse and longitudinal relaxivities at 1.5 T; c) and d) transverse and longitudinal relaxivities at 9.4 T.

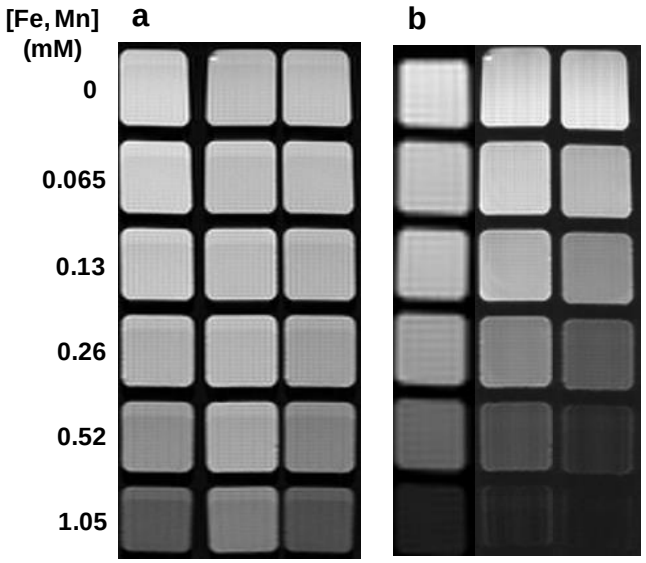

Figure S9. In vitro T_1 (a) and T_2 (b) weighted MRI at 9.4 T of Neutral, Positive and Zwitterionic magnetic nanoparticles, respectively.

5. Cytotoxicity assays and *in vivo* weight control.

Two different techniques were performed in order to assess the cell activity after exposure to functionalized magnetic nanoparticles. On one hand, the cell metabolic activity was evaluated using the MTT assay. And on the other hand, the integrity of the membrane was measured by the LDH assay. Mouse microglial cell line (N13) was selected as a working model. The cultured cells were exposed to increasing concentration of different functionalized MNPs from 0.1 μg/mL to 100 μg/mL for 24 h, giving as result that the exposure to MNP with different superficial charges did not produce a significant decay in mitochondrial activity in any case ($p<0.05$, U Mann-Whitney Test). Similarly, the exposure to MNP did not produce an increasing in extracellular LDH. Summarizing, both assays showed no cytotoxicity effects after 24 h of incubation with charged magnetic nanoparticles in either at mitochondrial activity level or at membrane integrity level.

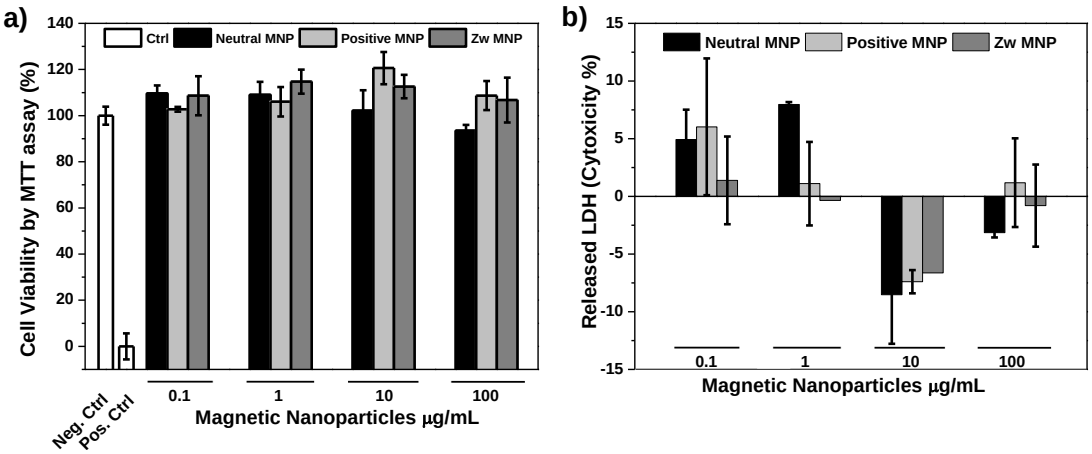

Figure S10. Cytotoxicity assays of charged magnetic nanoparticles on N13 cells treated for 24 h: a) by MTT assay and b) by LDH assay at different concentrations.

The possible side effects in mice provoked by the exposition to magnetic nanoparticles were also evaluated by analyzing the weight gain or weight loss of the mice, and by histological analysis of the main organs, namely, liver, kidneys, spleen, lungs and brain, after 1 h of magnetic nanoparticles administration. It is known that the subsequent weight gain or loss after a treatment with nanoparticles or other chemical substances could be due to acute internal damages in the main organs.

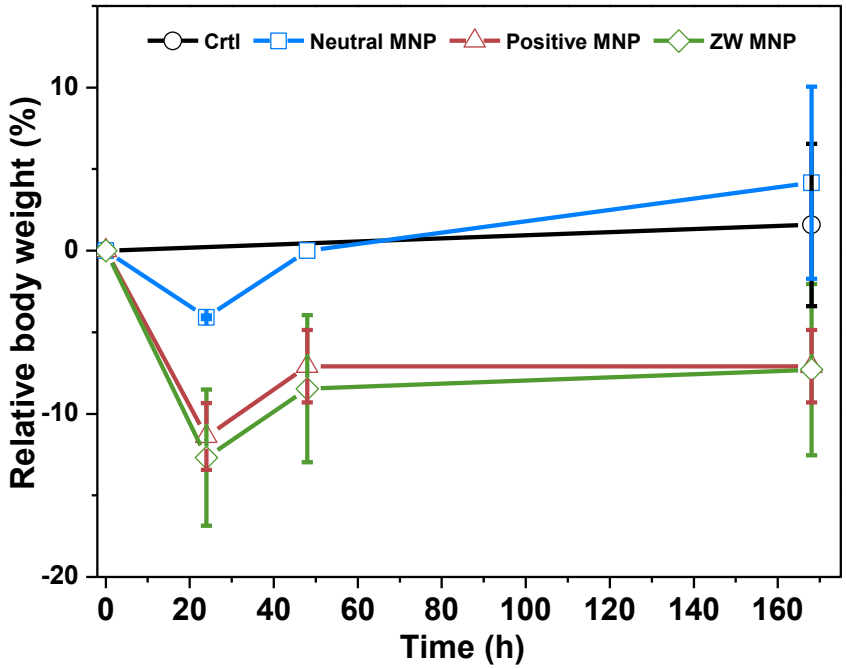

Figure S11. Weight profile of intravenously injected magnetic nanoparticles in mice and non-injected mice (control).

In vitro cell uptake of functionalized magnetic nanoparticles in N13 cell line.

The cellular uptake may serve to give information on both toxicity (the higher uptake increased toxicity of the MNPs) and the clearance of the MNPs from the bloodstream in *in vivo* experiments. In this case, since the cell toxicity is almost zero, the *in vitro* experiments give us a preliminary idea of how the MNPs interacts with the MPS, once

the MNPs are injected into the animal models. The uptake of the MNPs by N13 cells is clearly time-dependent, being the order of uptake Neutral < Positive < Zwitterionic.

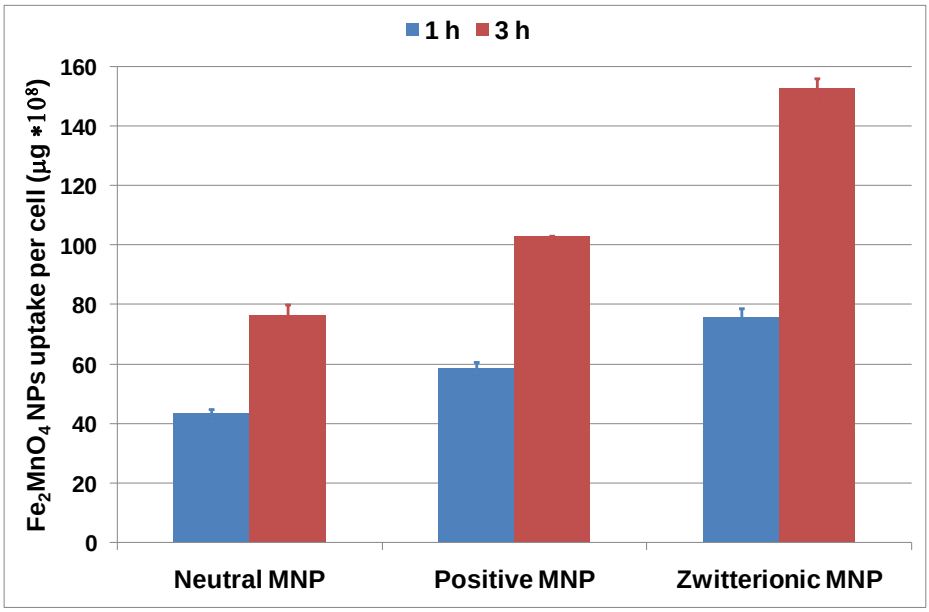

Figure S12. In vitro uptake of the MNPs (Neutral, Positive and Zwitterionic) by N13 cells at 1 h (blue) and 3 h (red grey).

6. Magnetic Resonance Images of liver, kidneys, spleen and muscle at different times.

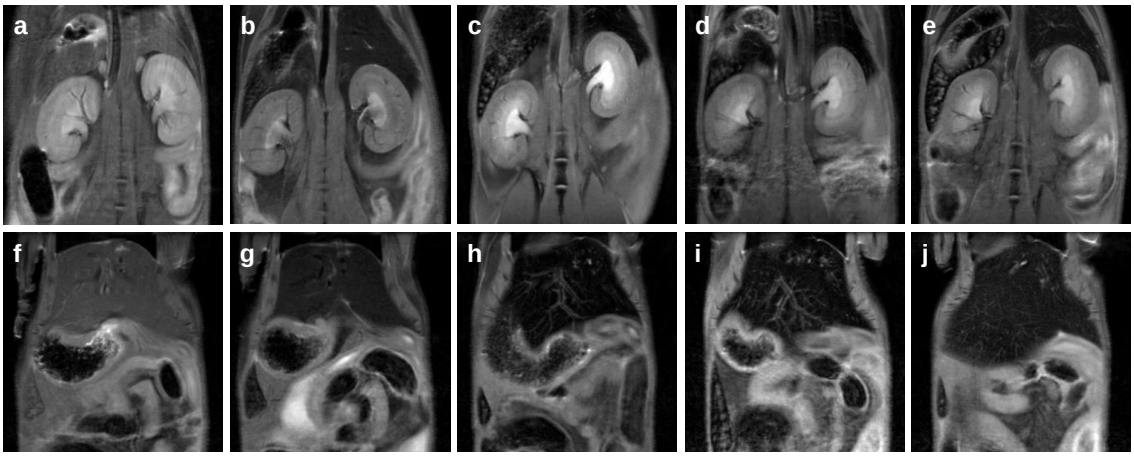

Figure S13. Representative T_2-weighted MR images at different experimental times after the intravenous injection of Neutral magnetic nanoparticles. a-e) T_2-weighted images of kidneys and muscle at 0, 1, 24, 48 and 168 h respectively after injection. f-h) T_2-weighted images of liver and spleen at 0, 1, 24, 48 and 168 h after injection.

Neutral MNP	T_2 (ms)				ΔT_2 (ms)			
	Liver	Kidneys	Spleen	Muscle	Liver	Kidneys	Spleen	Muscle
0	20.9	47.5	24	23.7	0	0	0	0
1	11.3	29.2	16.7	22.8	-9.6	-18.3	-7.3	-0.9
24	15.8	39.8	26.2	26	-5.1	-7.7	2.2	2.3
48	18.5	41.4	26.6	28.2	-2.4	-6.1	2.6	4.5
168	14.4	47.5	27.6	25	-6.5	0	3.6	1.3

Supplementary Table 1. T_2 quantitative averages and ΔT2 values of liver, kidneys, spleen and muscle at different times after intravenous injection of neutral MNPs. The average values were obtained by performing three experiments.

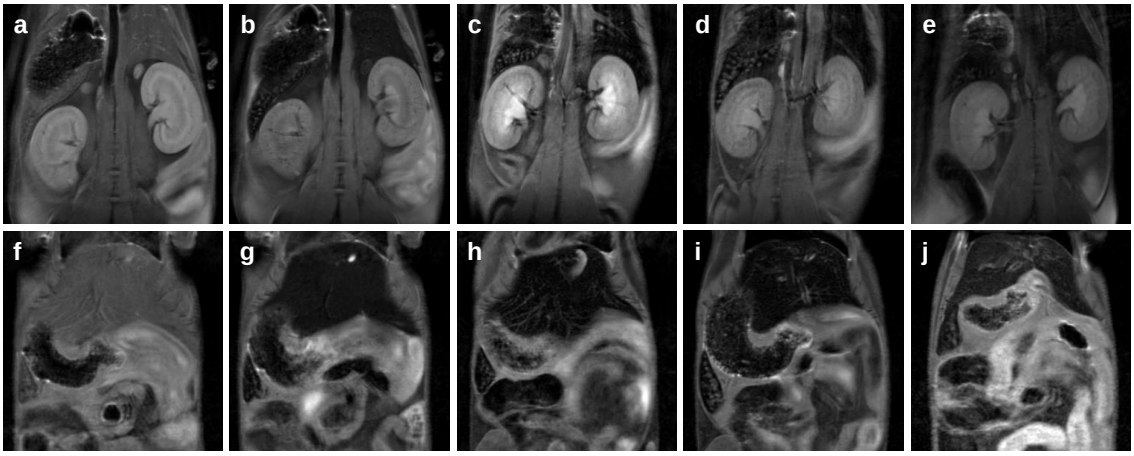

Figure S14. Representative T_2-weighted MR images at different experimental times after the intravenous injection of Positive magnetic nanoparticles. a-e) T_2-weighted images of kidneys and muscle at 0, 1, 24, 48 and 168 h respectively after injection. f-h) T_2-weighted images of liver and spleen at 0, 1, 24, 48 and 168 h after injection.

Positive MNP	T_2 (ms)				ΔT_2 (ms)			
	Liver	Kidneys	Spleen	Muscle	Liver	Kidneys	Spleen	Muscle
0	18.7	50.2	22.3	22.8	0	0	0	0
1	10.5	38	14.5	23.5	-8.2	-12.2	-7.8	0.7
24	20.1	46.1	26.3	22.8	1.4	-4.1	4	0
48	23.5	47.3	23.7	23.9	4.8	-2.9	1.4	1.1
168	21.7	50.4	23.7	23.1	3	0.2	1.4	0.3

Supplementary Table 2. T_2 quantitative averages and ΔT2 values of liver, kidneys, spleen and muscle at different times after intravenous injection of positive MNPs. The average values were obtained by performing three experiments.

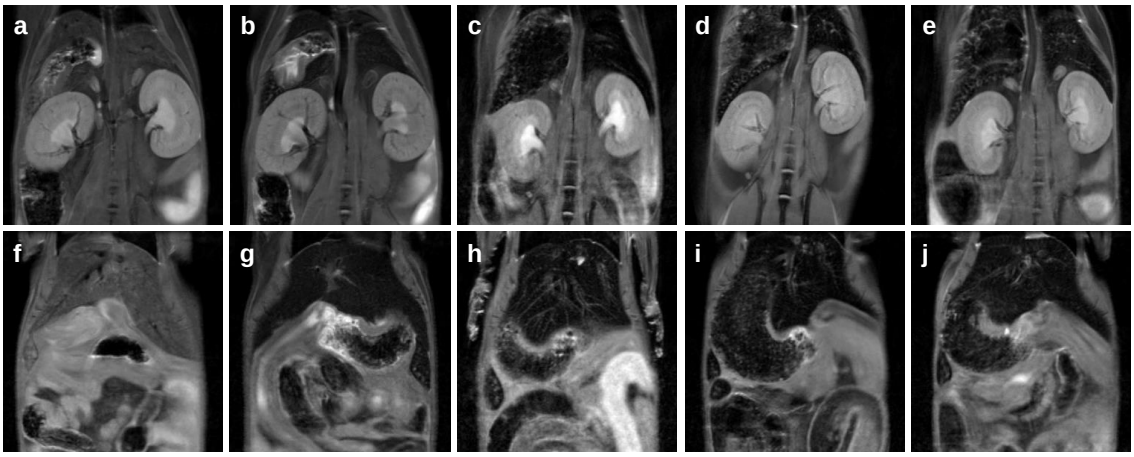

Figure S15. Representative T_2-weighted MR images at different experimental times after the intravenous injection of Zwitterionic magnetic nanoparticles. a-e) T_2-weighted images of kidneys and muscle at 0, 1, 24, 48 and 168 h respectively after injection. f-h) T_2-weighted images of liver and spleen at 0, 1, 24, 48 and 168 h after injection.

Zw MNP	T_2 (ms)				ΔT_2 (ms)			
	Liver	Kidneys	Spleen	Muscle	Liver	Kidneys	Spleen	Muscle
0	20.5	49.1	23.9	23.3	0	0	0	0
1	11.5	36.1	12	23.3	-9	-13	-11.9	0
24	20.8	40.6	23.8	22	0.3	-8.5	-0.1	-1.3
48	21.7	43.1	25.1	23.9	1.2	-6	1.2	0.6
168	20.4	46.5	23.6	24.2	-0.1	-2.6	-0.3	1.1

Supplementary Table 3. T_2 quantitative averages and ΔT2 values of liver, kidneys, spleen and muscle at different times after intravenous injection of positive MNPs. The average values were obtained by performing three experiments.

7. In vivo pharmacokinetics after MNP administration

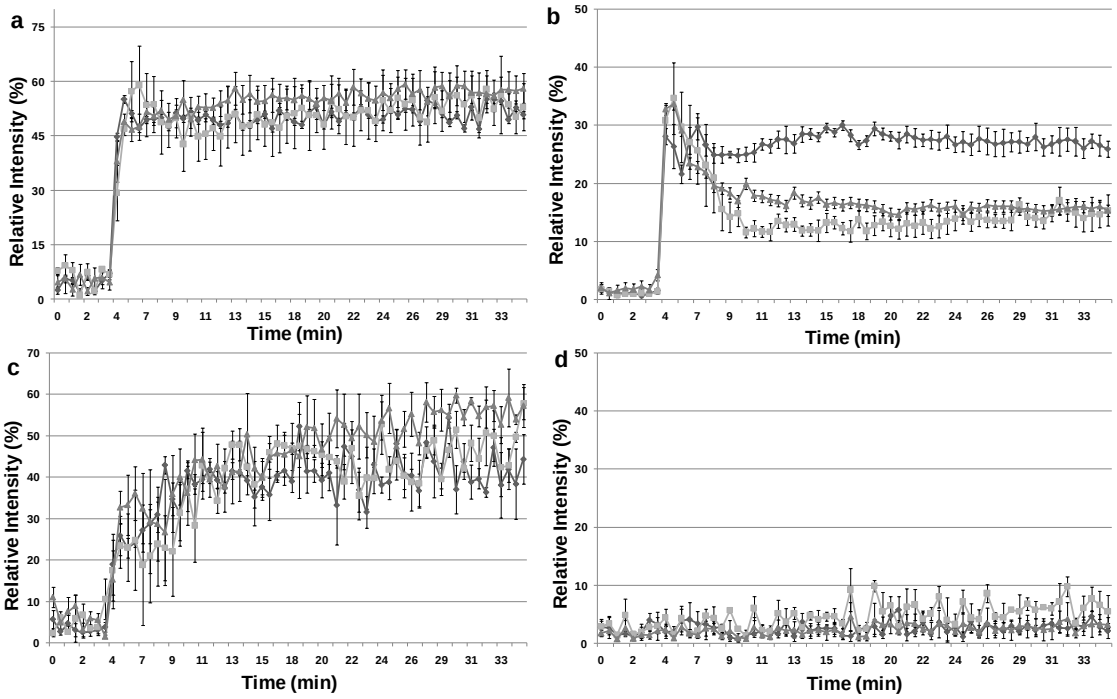

Figure S16. *In vivo* time courses of neutral MNPs (diamonds), positive MNPs (squares) and zwitterionic MNPs (triangles) after being intravenously injected in balb/c mice: a) Liver; b) Kidneys; c) Spleen and d) Muscle.

8. Histology of mouse after MNP injection.

The histology of the major organs was determined by light microscopy. The tissues were fixed in 4% Formaldehyde (Panreac, pH 7 buffered) for 48 h, changing the 4% Formaldehyde after 24 h. Then, the samples were dehydrated through graded ethanol, and embedded in paraffin (temperature 56 ºC for 2 h under stirring and vacuum). At this point, samples from the different organs were stained with Haematoxylin and Eosin (H&E) to assess tissue architecture, and liver and spleen were also stained with Prussian Blue to visualize iron deposits. The detailed procedures are described below.

Haematoxylin and Eosin (H&E): the paraffin-embedded samples were sectioned at 7 μm thickness and then were deparaffinized, rehydrated and stained with H&E, then

dehydrated in ascending concentrations of ethanol, cleared in xylene and mounted in commercial glass slide.

Prussian Blue (PB): the paraffin-embedded samples were sectioned at 7 µm thickness and then were deparaffinized, rehydrated, submerged in 20% hydrochloric acid and 10% potassium ferrocyanide, washed with water and counterstained with Nuclear Fast Red, dehydrated in ascending concentrations of ethanol, cleared in xylene and mounted in commercial glass slide.

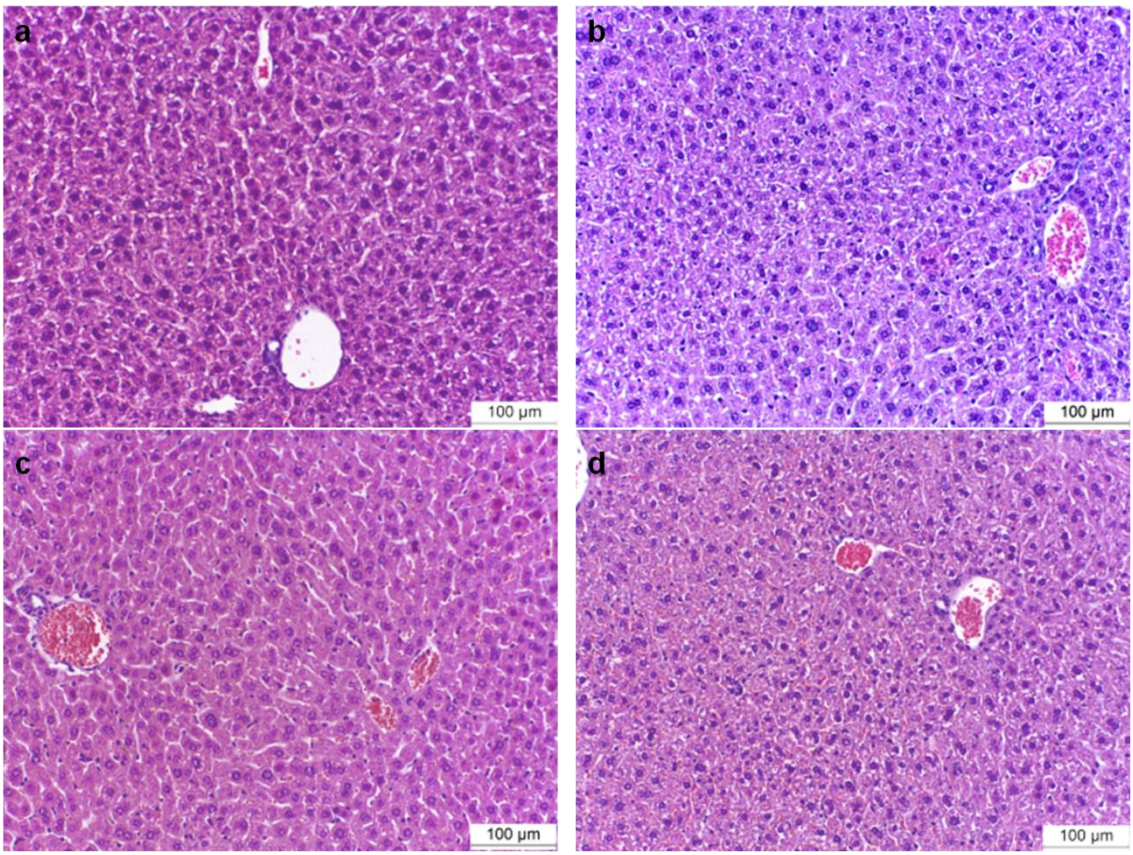

Figure S17 Histological analysis of the liver tissue stained with H&E in control (a), and intravenously injected mice: neutral MNP (b); positive MNP (c) and zwitterionic MNP (d).

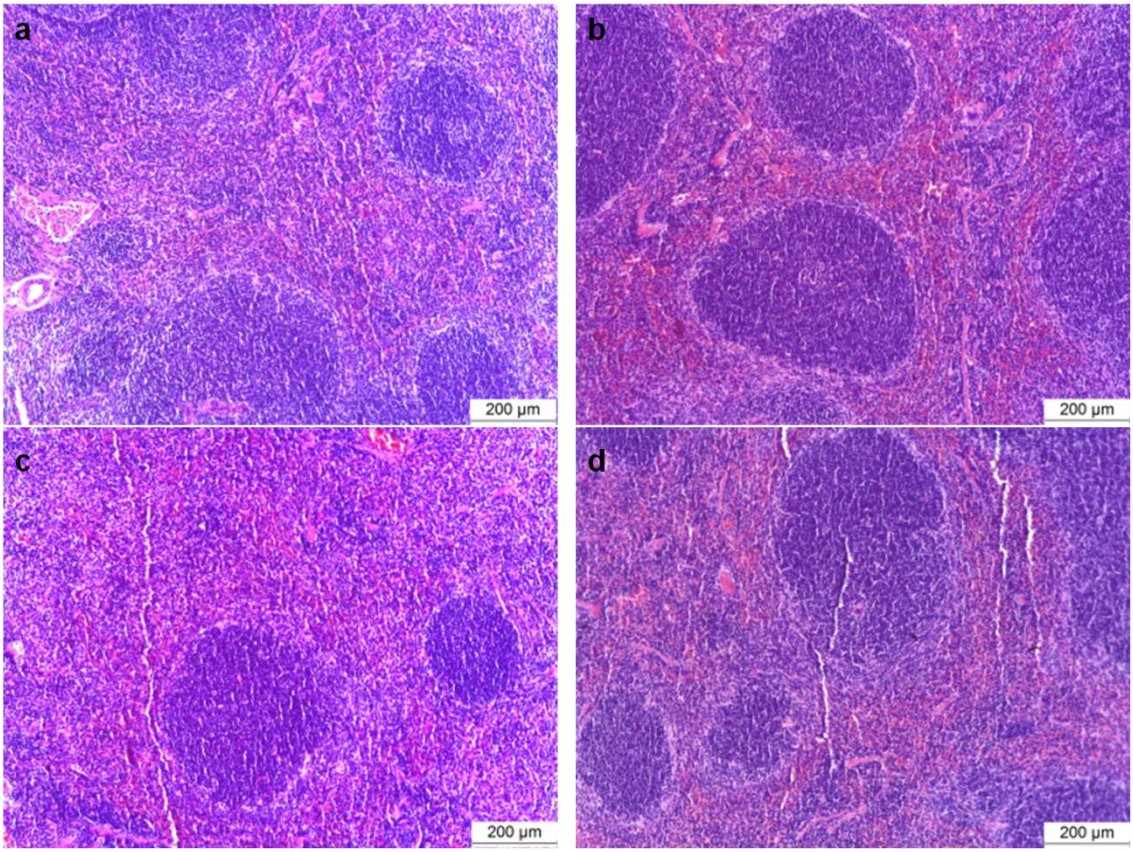

Figure S18. Histological analysis of the spleen tissue stained with H&E in control (a), and intravenously injected mice: neutral MNP (b); positive MNP (c) and zwitterionic MNP (d).

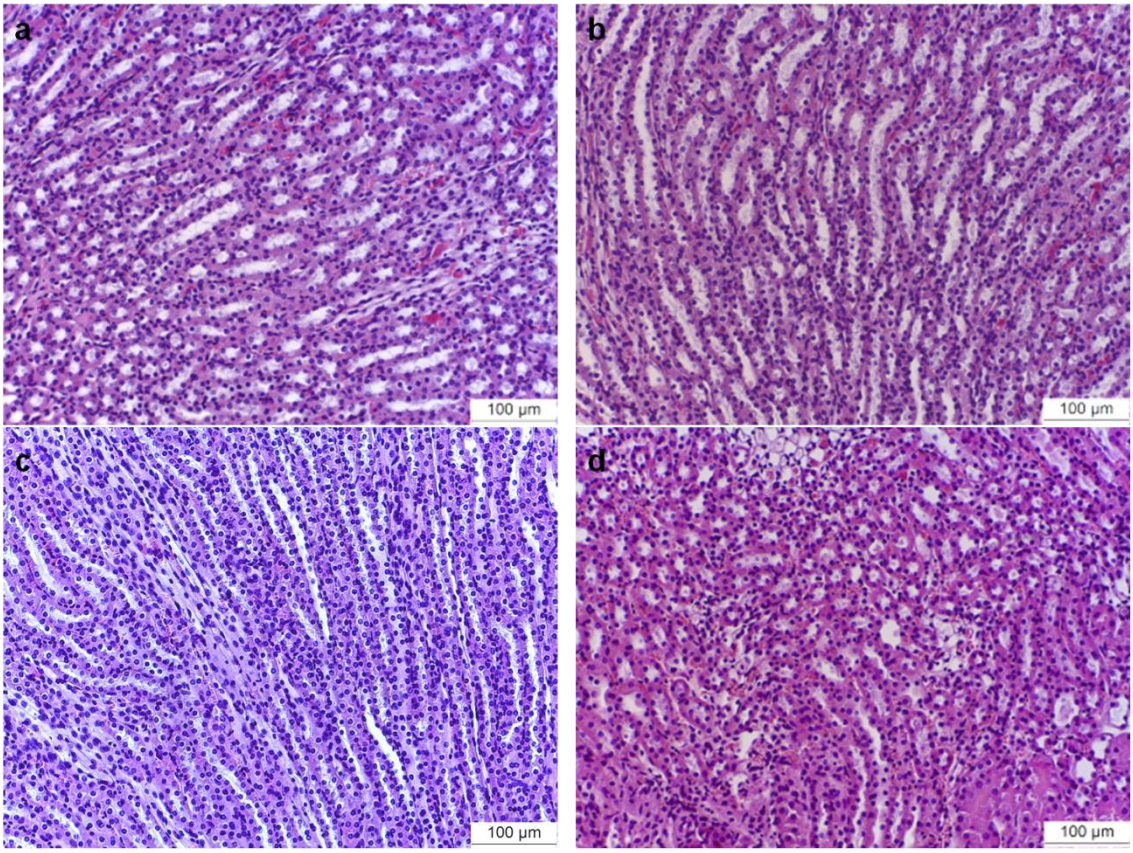

Figure S19. Histological analysis of the renal medulla tissue stained with H&E in control (a), and intravenously injected mice: neutral MNP (b); positive MNP (c) and zwitterionic MNP (d).

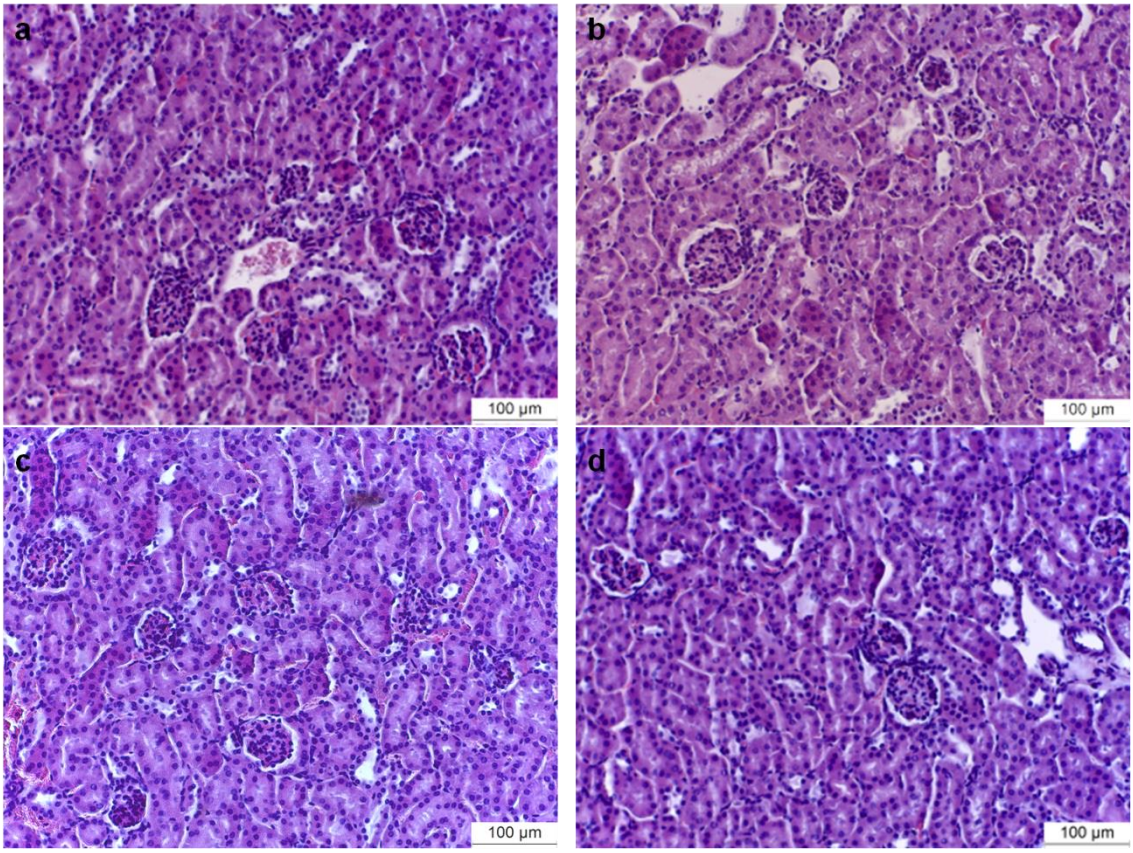

Figure S20. Histological analysis of the renal cortex tissue stained with H&E in control (a), and intravenously injected mice: neutral MNP (b); positive MNP (c) and zwitterionic MNP (d).

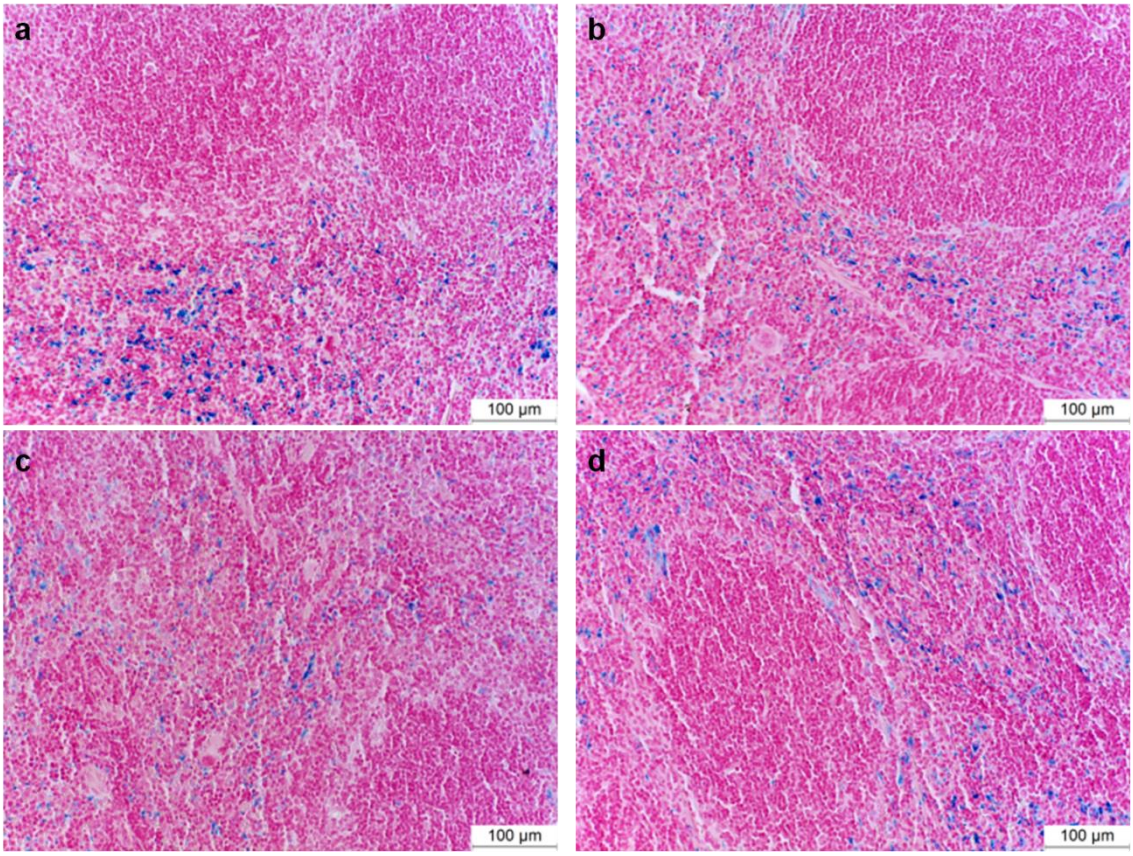

Figure S21. Histological analysis of the spleen tissue stained with Prussian Blue in control (a), and intravenously injected mice: neutral MNP (b); positive MNP (c) and zwitterionic MNP (d).

1. S. Sun, H. Zeng, D. B. Robinson, S. Raoux, P. M. Rice, S. X. Wang and G. Li, *Journal of the American Chemical Society*, 2004, 126, 273-279.
2. M. Pernia Leal, S. Rivera-Fernández, J. M. Franco, D. Pozo, J. M. De La Fuente and M. L. García-Martín, *Nanoscale*, 2015, 7, 2050-2059.
3. N. Zhan, G. Palui and H. Mattoussi, *Nature Protocols*, 2015, 10, 859-874.
4. M. P. Leal, C. Muñoz-Hernández, C. C. Berry and M. L. García-Martín, *RSC Advances*, 2015, 5, 76883-76891.